


FULL PAPER

Open Access



Ionospheric disturbances over South America related to Tonga volcanic eruption

H. Takahashi^{1*} , C. A. O. B. Figueiredo¹, D. Barros¹, C. M. Wrasse¹, G. A. Giongo¹, R. H. Honda¹, L. F. R. Vital¹, L. C. A. Resende^{1,2}, P. K. Nyassor¹, T. T. Ayorinde¹, C. S. Carmo², M. B. Padua¹ and Y. Otsuka³

Abstract

On January 15, 2022, we observed various unusual atmospheric wave events over South America: Atmospheric pressure waves (Lamb mode) around 12:30 to 17:30 UT, tsunamis along the Chilean coast at around 17:00 to 19:00 UT, and ionospheric disturbances between 11:30 and 20:00 UT. We understand that these events were generated by the Tonga volcanic eruption that occurred at (20.55°S, 175.39°W) in South Pacific Ocean at 04:15 UT. Several traveling ionospheric disturbances (TIDs), the horizontal wavelengths of 330 to 1174 km and the phase speed of 275–544 m/s were observed before and after the Lamb wave passed over the continent and the arrival of the tsunami on the Chile coast. The observed TID characteristics suggest us that these waves might be generated by the two atmospheric events, Lamb wave and gravity waves induced by the tsunamis. This is the first time to report the signature of ionospheric disturbances over the South American continent generated by the huge volcanic eruption.

Keywords Tonga volcanic eruption, Ionospheric disturbance, South America, Lamb wave, Tsunami

Plain Language Summary

A huge volcanic eruption occurred at the volcano Hunga Tonga Hunga Ha'apai (20.55°S, 175.39°W), one of the islands of the Tonga archipelago in the South Pacific Ocean, on 15 January 2022, at 04:15 UT (Universal Time). The eruption released a huge amount of thermal energy into the atmosphere that reached up to ~50 km altitude. Such an explosive release of thermal energy produced atmospheric pressure waves, acoustic waves, and internal gravity waves in the lower atmosphere propagating horizontally and vertically up to the ionosphere (above 200 km altitude). The present work, as the first time, reports signatures of the ionospheric disturbances caused by the tsunami and atmospheric pressure waves over the South American continent.

*Correspondence:

H. Takahashi

hisao.takahashi@inpe.br

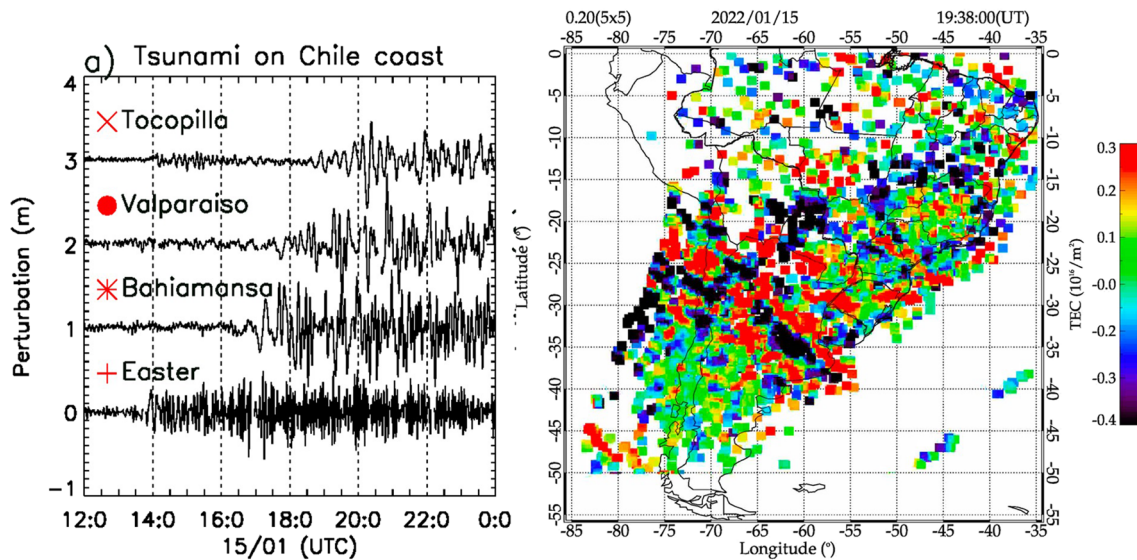
Full list of author information is available at the end of the article



© The Author(s) 2023. **Open Access** This article is licensed under a Creative Commons Attribution 4.0 International License, which permits use, sharing, adaptation, distribution and reproduction in any medium or format, as long as you give appropriate credit to the original author(s) and the source, provide a link to the Creative Commons licence, and indicate if changes were made. The images or other third party material in this article are included in the article's Creative Commons licence, unless indicated otherwise in a credit line to the material. If material is not included in the article's Creative Commons licence and your intended use is not permitted by statutory regulation or exceeds the permitted use, you will need to obtain permission directly from the copyright holder. To view a copy of this licence, visit <http://creativecommons.org/licenses/by/4.0/>.

Graphical Abstract

Tonga volcanic Eruption and South America



Introduction

On 15 January 2022 at 04:15 UT a large under-water volcanic eruption occurred at Hunga Tonga Hunga Ha'apai (20.55°S, 175.39°W) in the archipelago of Tonga (hereafter Tonga eruption), South Pacific Ocean. National Oceanic and Atmospheric Administration (NOAA/USA), informed that the gas released explosively reached 40 km altitude, and the atmospheric pressure wave left from the center of eruption expanded radially as a mode of Lamb wave (Duncombe 2022). Simultaneously a variety of acoustic and gravity waves propagated to the upper atmosphere and ionosphere (Wright et al. 2022; Themens et al. 2022; Zhang et al. 2022). Tsunamis were also generated and propagated on the Pacific Ocean (see "data availability").

Ionospheric disturbances during significant atmospheric events such as earthquakes, tsunamis and volcanic eruptions have been extensively studied (e. g., Komjathy et al. 2016; Astafyeva 2019). Especially the recent Tohoku earthquake on 11 March 2011 generated a large amplitude of tsunamis, and subsequent ionospheric disturbances were observed by several research groups (Tsugawa et al. 2011; Makela et al. 2011; Smith et al. 2015; Azeem et al. 2017). In the case of volcanic eruptions, the Earth's atmosphere would be further affected by the different kind of disturbances. The explosive release of high temperature volcanic gas into the troposphere produces atmospheric pressure waves. It

propagates radially between the ground surface and the troposphere as a Lamb wave (Lindzen and Blake 1972). Lamb wave propagates by a non-dispersive mode with a local speed of sound ~ 310 m/s. Although the propagation is confined in the troposphere, a part of wave oscillation leaks to the mesosphere and the lower thermosphere (Nishida et al. 2014). In the Tonga eruption, Wrights et al. (2022) showed a concentric Lamb wave from the Tonga Eruption area. The concentric wave structure of the temperature field in the stratosphere was observed by Atmospheric Infrared Sounder (AIRS) mounted on the Aqua satellite (Adam 2022).

Ionospheric disturbances caused by the last Tonga eruption were quickly reported by Zhang et al. (2022) and Lin et al. (2022). Themens et al. (2022), using GNSS ground receiver data, identified the large scale Traveling Ionospheric Disturbances (LSTIDs), horizontal wavelength longer than 1000 km near the Tonga eruption area, and Medium Scale TID (MSTIDs), horizontal wavelength between 350 and 950 km away from the eruption region. Lin et al. (2022) showed concentric TIDs driven by the Tonga eruption in geomagnetically conjugate points, Australia and Japan. The global scale ionospheric disturbances, nowadays, can be monitored by the Global Navigation Satellite System (GNSS) and ground-based GNSS receiver systems. The present work aims to report the ionospheric disturbances after the Tonga eruption observed by the GNSS receiver

network in the South American sector. The passage of Lamb waves over the continent and the arrival of the Tsunami on the coast of Chile, and the ionospheric disturbances are presented.

Observations

In the present work, we observed the atmospheric pressure variation by the barometer data, sea surface level variation by the Tsunami sensor buoy data, and the ionospheric disturbance by the ground-based GNSS receiver data. Measurements of the ground-level atmospheric pressure have been carried out by worldwide GNSS ground-based meteorological stations. The data collection frequency is 1/min. The data from the Brazilian side are available in the RBMC (Rede Brasileiro de Monitoramento Contínuo) of IBGE (Instituto Brasileiro de Geografia e Estatística) (see “data availability”). The data from the Chilean meteorological stations are also available (see “data availability”).

Data of the ocean sea surface level were obtained from the Global Sea level Observing System (GLOSS/UNESCO) (see “data availability”). The data collecting frequency is 1/min. In the present work, we used three monitoring sites along the Chilean coast ($\sim 72^\circ\text{W}$) and one at Easter Island (27.2°S , 109.4°W). The tsunami arrival time and the amplitude of oscillation of the sea level are used.

Total Electron Content (TEC) is obtained from the GNSS receiver data, which are available in the website RBMC/IBGE (see “data availability”). Ionospheric Total Electron Content (TEC) can be obtained by using a phase difference between the two carrier frequencies of the GNSS satellite. One TEC unit corresponds to 10^{16} electrons/(m^2 column). Normally, the amplitude of disturbance of TEC in the ionosphere by the Travelling Ionospheric Disturbances (TIDs) is less than one TEC unit (Otsuka et al. 2013). In order to detect such a small amplitude of variation, we used detrended TEC (dTEC), which is defined at a time “ t ” as

$$(\text{dTEC})_t = (\text{TEC})_t - \langle \text{TEC}(t \pm 30 \text{ min}) \rangle,$$

where $\langle \rangle$ indicates a running average of 1-min TEC values for ± 30 min. The procedure of TEC and dTEC calculations have been reported elsewhere (Otsuka et al. 2013; Figueiredo et al. 2018). After illustrating a dTEC-map, keograms are made plotting longitudinally (latitudinally) sliced dTEC maps as a function of time, by which TID wave fronts can be better identified. The wave characteristics, wavelength, period, phase speed and propagation direction can be obtained by using FFT spectral analysis of the keograms (Figueiredo et al. 2018).

Results

Atmospheric pressure (Lamb) wave

The Lamb wave reached the south of Chile at Futaleufu: SCFT(43.2°S , 71.9°W) at 12:29 UT with the amplitude of ± 1.0 hPa. Figure 1a shows temporal variations of the ground level atmospheric pressure measured at 4 observation sites from Chile to Brazil on 15 January 2022. After the arrival of the Lamb wave at SCFT on 12:29 UT, it arrived at Santa Maria: SMAR (29.7°S , 53.7°W) at 14:38 UT, Franca: SPFR (20.5°S , 47.4°W) at 15:38 UT, and Fortaleza: CEEU (3.9°S , 38.4°W) in the low latitude region at 17:29 UT. The Lamb wave took around 5.0 h to cross the South American continent from SW to NE. Also in Fig. 1, the second wave paths can be seen from 03:00 to 08:00 UT on 16 January 2022. The phase velocity and propagation direction of the Lamb wave over the South American continent were obtained from the time delay between the observation sites. In this calculation we used 30 ground-based GNSS meteorological sites that have an atmospheric pressure sensor (barometer). Figure 1b shows the relation between the longitudinal and latitudinal distances measured from a reference point at (45.92°S , 71.68°W) and the time delay of the peak occurrence of the observation sites. The phase speed obtained from the linear relation of the plots is 304.5 ± 5.6 m/s. It is close to that reported by Kubota et al. (2022), which is ~ 300 m/s, but a little slower than that was observed near the South Pacific region, 318 m/s (Wright et al. 2022). This difference could be due to the local propagation condition of such as the background wind fields and the topography of South American continent (Wright et al. 2022). The azimuth of the direction of propagation was $46.7^\circ(\text{NE})$. If we consider the phase speed, ~ 0.31 km/s, the direction of propagation and the difference of occurrence time between the Tonga eruption and Futaleufu, ~ 8.30 h, the wave travelling distance is about 9300 km, which is close to the surface distance between the two locations. This observational evidence suggests us that the Lamb wave started from the Tonga eruption, propagating by a concentric form, reaching the antipodal point in North Africa, and continued to the second path (Matoza et al. 2022).

Tsunami

The arrival of tsunami on the southern coast of Chile is shown in Fig. 2. It presents the temporal variation of sea surface measured by buoy as mentioned in the previous section. A high-pass filter with a 120 min window was applied to take longer period (tidal) oscillations out. It is clear to identify the arrival of the tsunami wave at Easter island (27.2°S , 109.4°W) at 13:50 UT. Along the Chilean coast, it arrived at Bahia Mansa (40.6°S , 73.7°W) at 17:15

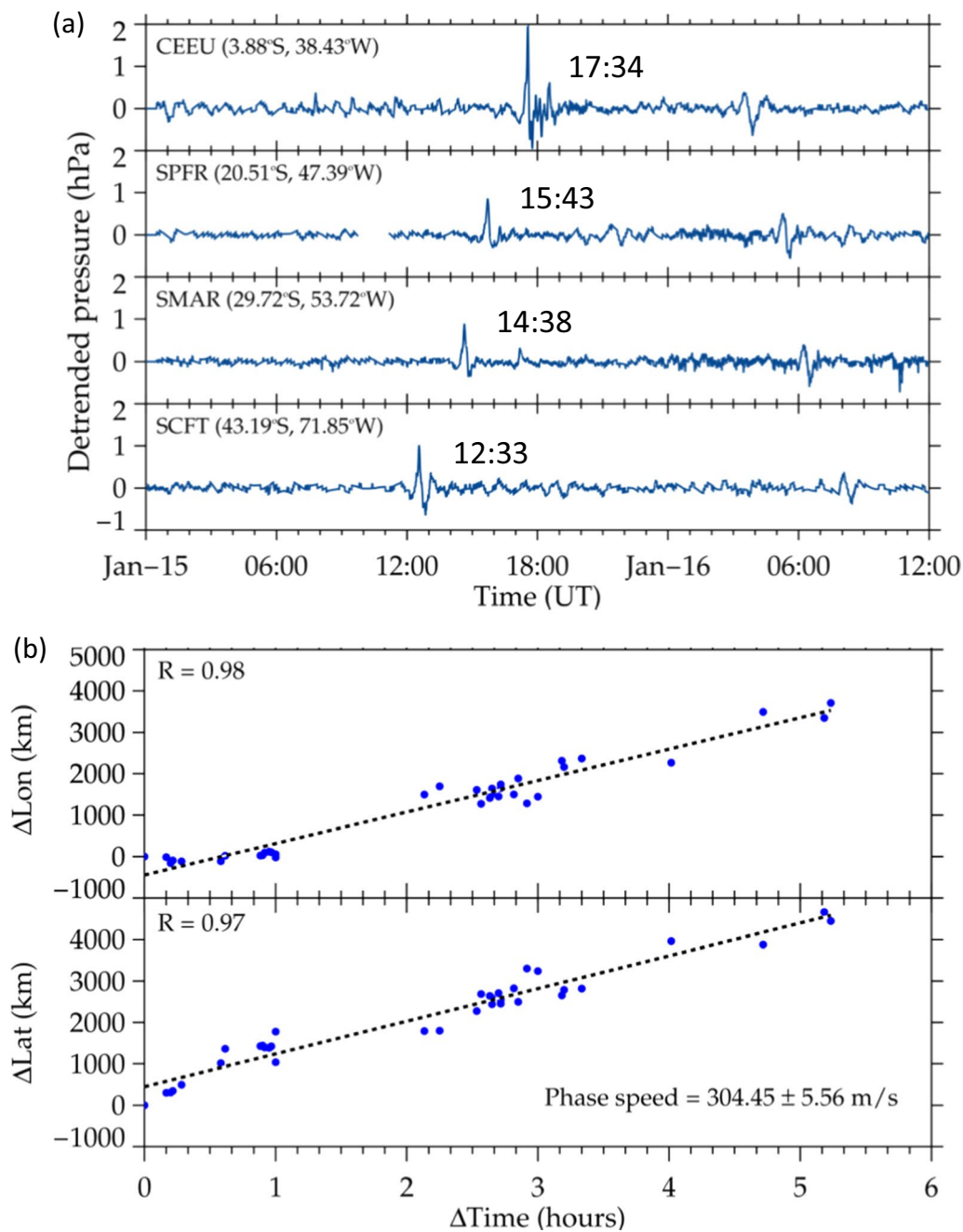


Fig. 1 Atmospheric pressure observation over South America: (a) Occurrence of the Lamb wave at 4 locations, (b) Longitudinal (top) and latitudinal (down) time delays between the 30 observation sites over South America (Chile and Brazil)

UT, followed by Valparaiso (33.0°S, 71.6°W) and Tocopilla (22.1°S, 70.2°W) at around 18:00 UT. One can notice that the tsunami wave first arrived at the south of the Chilean coast and then went to the middle to low latitudes. The period of oscillation of the sea surface is somewhat short around 12 min (at Easter). At Bahia Mansa, the period is long, 20 to 30 min in the beginning at around 17:00 UT,

then became shorter (11 min). The amplitude of oscillation (peak to peak) was 46 cm at Easter, 100 cm at Bahia Mansa, and 20 to 50 cm at Valparaiso to Tocopilla in the middle to low latitudes. The amplitude of oscillation is dependent on the landscape of the coast, too. Global scale simulation of the tsunami waves showed the first arrival of the tsunami on the southern coast of Chile (see

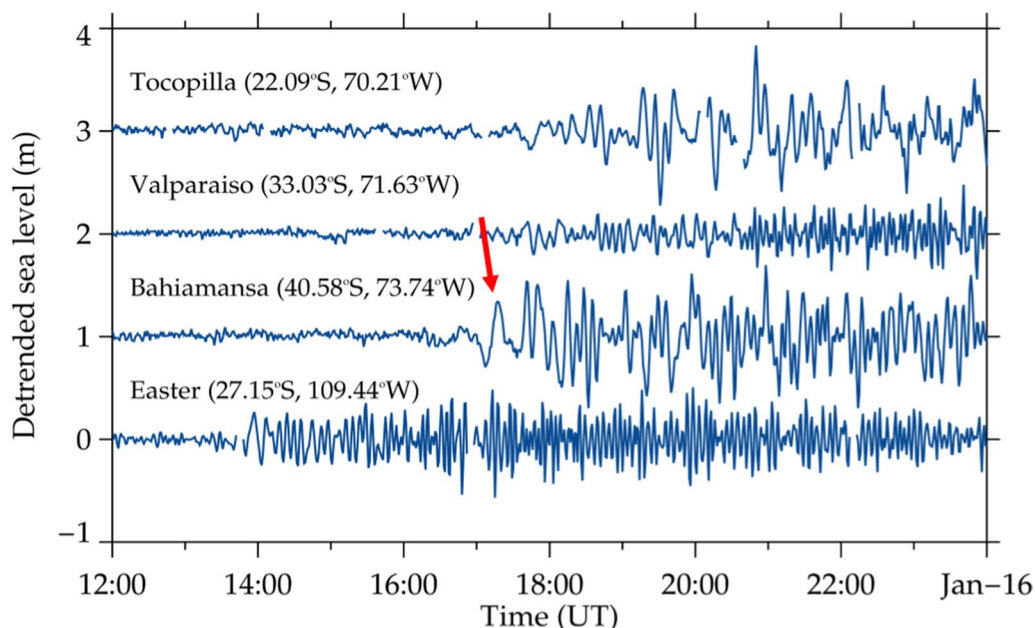


Fig. 2 Tsunami induced sea surface oscillation observed at Easter island, Bahia Mansa, Valparaiso and Tocopilla at the Chilean coast on 15 Jan 2022. The red arrow indicates the first arrival of tsunami

“data availability”). The wave characteristics of the Lamb wave and the Tsunami are summarized in Table 1.

Ionospheric disturbances

The ionospheric variabilities during the period of 15–16 January 2022 were monitored by observing spatial variability of the dTEC and ionograms. A variety of ionospheric disturbances (TIDs) was detected which were starting from the south of Chile (50°S, 75°W) at around 11:30 UT. In total we could identify nine TID wave events during the interval from 11:30 to 20:30 UT, those are presented in the following sections.

Chile 11:30–12:30 UT

A long wave TID can be seen in the south of the Chilean coast which started at around 11:30 UT propagating toward the SE direction. Figure 3a shows the dTEC map at 11:43 UT. The blue circle highlights the wave structures, extending the wave fronts from NE to SW. The wave characteristics were calculated by using a sequence of the dTEC maps and keograms as mentioned in the previous section. The results are listed in Table 1 as TID-1. The long wavelength (1174 km) and the fast phase velocity (544 m/s) indicate that it is a large scale TID (LSTID). Nearly overlapping to

Table 1 Wave characteristics of Lamb wave, tsunami and 9 TIDs, observed over South America on 15 January 2022

Wave ID	(Lat, Lon) (deg)	Start at (UT)	λ_H (km)	τ (min)	CH (m/s)	θ (deg)	Amplitude
Lamb wave	SCFT (43.2S, 71.9W)	12:30	--	Solitary	304.5 ± 06	46.7	± 1.0 hPa
Tsunami	BHM (40.6S, 73.7W)	17:15	--	32, 26, 12	--	--	± 30 cm
TID-1	30–40S (Chile)	11:30	1174 ± 117	36 ± 1	544 ± 56	139 ± 5	± 0.3 TECu
TID-2	30–40S (Chile)	11:45	946 ± 95	36 ± 2	438 ± 50	37 ± 4	1.5/– 0.3 TECu
TID-3	40–45S (Chile)	12:30	479 ± 88	20 ± 5	399 ± 124	32 ± 5	± 0.6 TECu
TID-4	35–40S (chile)	13:15	348 ± 6	19.7 ± 2	294 ± 26	40 ± 3	± 0.6 TECu
TID-5	30–40S (Chile)	16:05	875 ± 41	31 ± 01	470 ± 27	30 ± 2	± 2.5 TECu
TID-6	40–45S (Chile)	17:30	505 ± 70	24 ± 5	350 ± 88	24 ± 4	± 0.3 TECu
TID-7	35–40S (Chile)	18:35	330 ± 9	20 ± 0.8	275 ± 13	29 ± 2	± 0.3 TECu
TID-8	20–30S (Brazil)	15:31	366 ± 40	20 ± 2	305 ± 45	41 ± 5	± 0.6 TECu
TID-9	20–30S (Brazil)	19:00	667 ± 60	28 ± 3	397 ± 56	18 ± 6	+1.2/– 0.7 TECu

λ_H : horizontal wavelength, τ : period, C_H : phase speed, θ : azimuth of the propagation direction

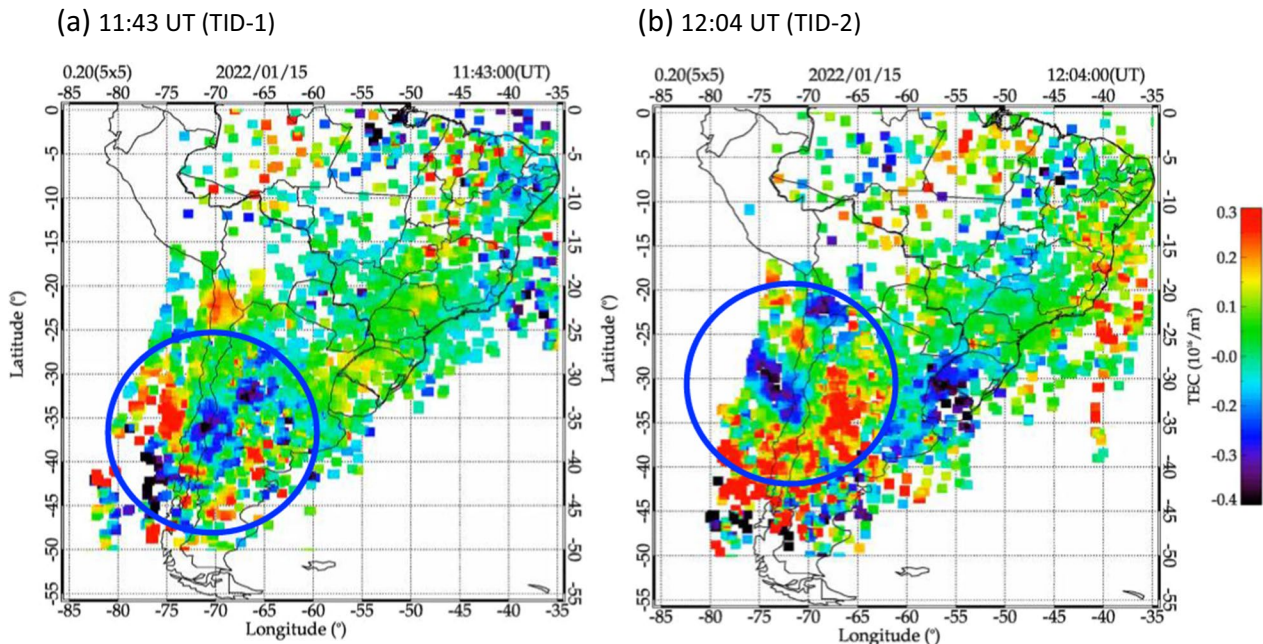


Fig. 3 Ionospheric dTEC map over South America on 15 Jan 2022: (a) TID-1 at 11:43 UT (highlighted by a blue circle), (b) TID-2 at 12:04 UT. The color bar shows the amplitude of dTEC oscillation

the LSTID, a second TID (TID-2) started at around 11:45 UT, which is shown in Fig. 3b. This is also a long (946 km) and fast (438 m/s) wave, but the propagation direction is toward NE, being different to TID-1. The wave characteristics of TID-2 are listed in Table 1. It should be noted that these two TIDs passed over the

Chilean coast almost 1 h before the passage of the Lamb wave. We will discuss on it in the next section.

Chile 12:30–13:30 UT

Figure 4a presents the dTEC map at 12:35 UT, which shows a wavefront (TID-3) in the south of Chile to

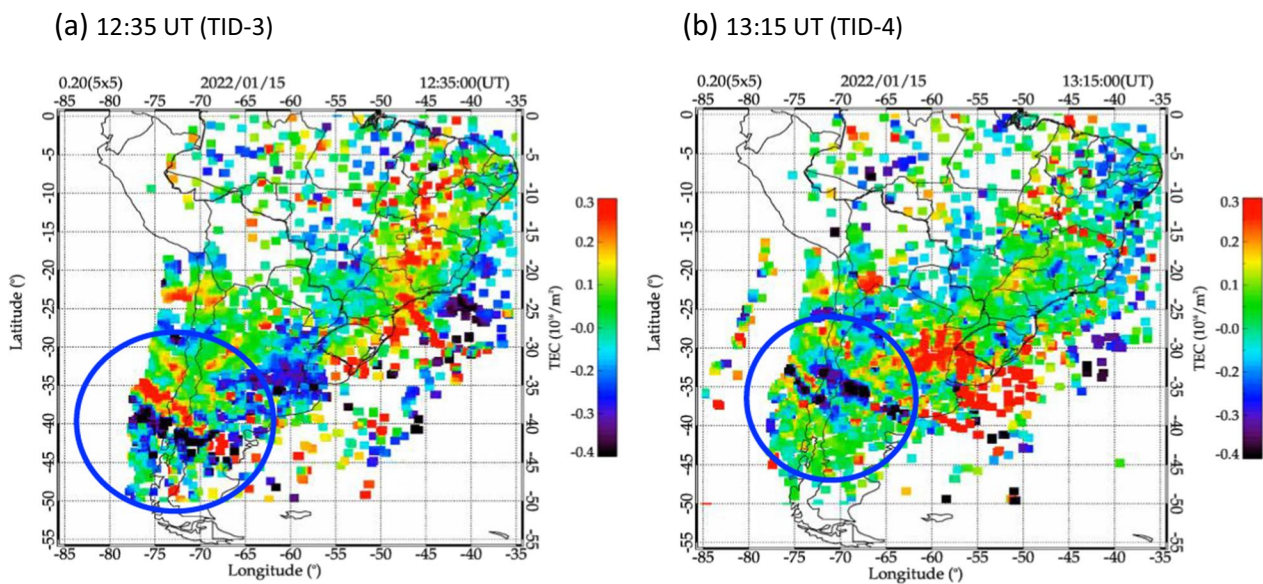


Fig. 4 Same as Fig. 3, except for (a) at 12:35 UT (TID-3) and (b) at 13:15 UT (TID-4)

Argentina (40°S, 75°W), highlighted by a blue circle in the figure. The wavefront is aligned from NW to SE moving toward NE, with the horizontal wavelength of 479 km and the phase speed of 399 m/s. Following to this wave, another wave (TID-4) with a shorter wavelength (348 km) and slow phase speed (294 m/s) appeared and propagated to the same direction with the TID-3. The wave characteristics of the two TIDs are presented in Table 1. It would be worth to point out that the appearance of TID-3 at 12:30 UT coincides with the arrival of

Lamb wave over the south of Chile. The propagation direction of the two TIDs, toward NE, is similar to the Lamb wave, and the phase speeds (294–399 m/s) are also similar to the Lamb wave (305 m/s).

Chile 16:00–17:00 UT

Between 14:00 and 16:00 UT, there was no significant wave propagation. On 16:05 UT a long wavelength (875 km) and a fast phase speed (470 m/s) TID was observed (named as TID-5). Figure 5 shows a snapshot at 16:34 UT. The propagation direction is similar to the earlier ones, toward 30°N. The amplitude of oscillation, however, is larger (2.5 TECu) compared to the others (0.3 TECu).

Chile 17:30–18:30 UT

At around 17:30 UT another wave structures started from the south, which are shown in Fig. 6. These are similar to the previous ones but forming several wavefronts propagating toward NE. Figure 6a is a snapshot of the wave structure at 17:38 UT, named as TID-6, highlighted by a blue circle. One can notice that there are longitudinally extended waves in the region of (40°S, 70°W) with the wavelength of 505 km and the phase speed of 350 m/s propagating toward NE. Also noticed that the wavefronts are a little curved form. Following to the TID-6, another but shorter wavelength (330 km), named TID-7, was observed in one hour later which highlighted by a blue circle in Fig. 6b. It seems that the TID-7 is a continuation of the TID-6 but reducing the horizontal wavelength

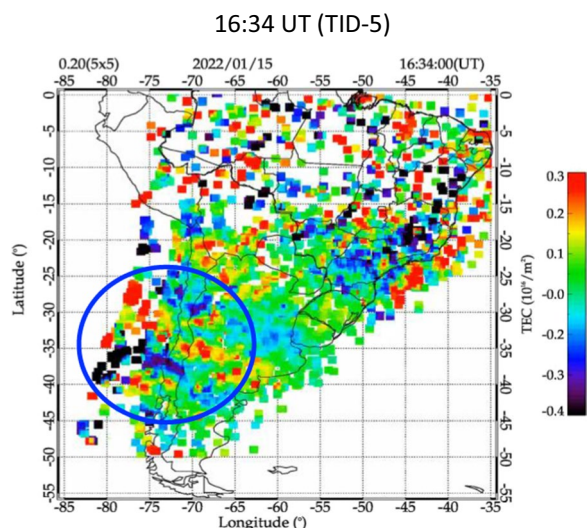


Fig. 5 Same as Fig. 3, except for 16:34 UT (TID-5)

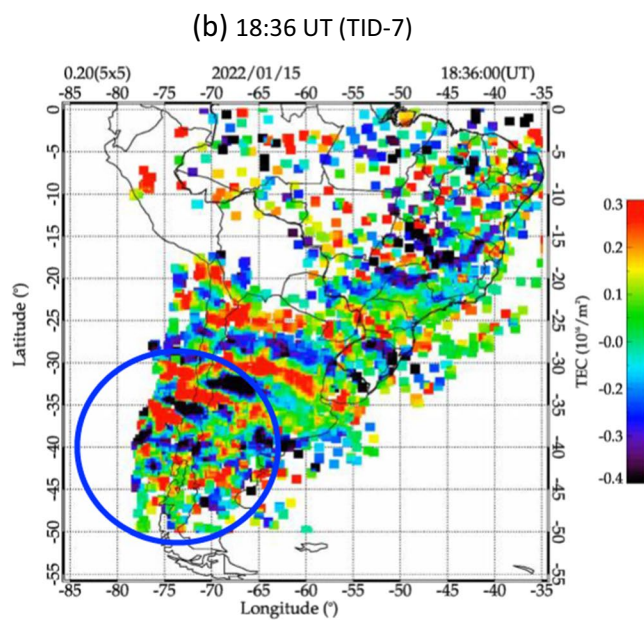
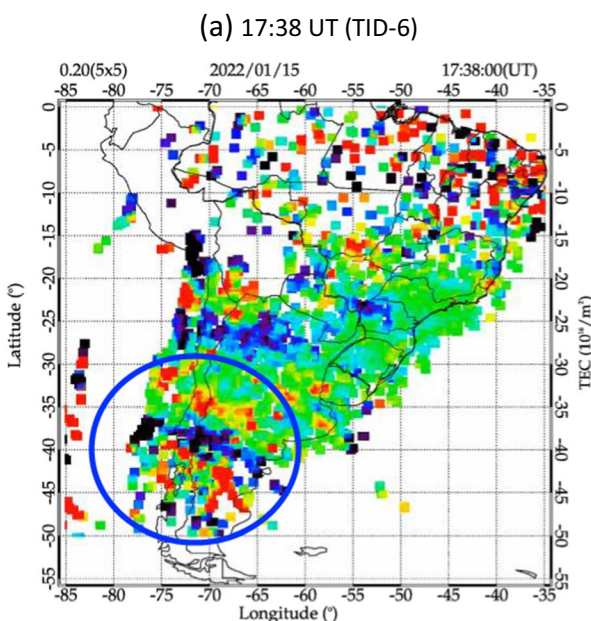


Fig. 6 Same as Fig. 3, except for (a) at 17:38 UT (TID-6) and (b) at 18:36 UT (TID-7)

and the phase speed. The longitudinally extended wave fronts at around 30°S, located at NE of the TID-7, are those observed in Fig. 6a and advanced toward NE in one hour. It looks that they have a concentric form. It should be noted here that the tsunami arrived at the Chilean coast at around 17:15 UT, which is 15 min earlier to the appearance of the TID-6.

Brazil 15:30 and 19:00 UT

All of the observed TIDs from the Chile side (TID-2 to TID-7), except TID-1, were propagating toward NE. In the low latitude region (in Brazil), we could identify two TIDs, TID-8 and TID-9, which are shown in Fig. 7. The TID-8 (λ_H : 366 km) was observed at around (20°S, 50°W) at 15:30 UT. This must be continuation of the TID-4 (λ_H : 348 km) observed at the Chile side at around 13:15 UT (Fig. 4). The TID-9 (λ_H : 667 km) observed at (25°S, 50°W) at 19:00 UT looks like a continuation of TID-6 (λ_H : 505 km) observed in the Chile side at around 17:38 UT. The wave characteristics of these TIDs are summarized in Table 1. It can be seen that TID-8 and TID-4, and TID-9 and TID-6, are same within the error ranges presented in Figs. 6 and 7. The propagation features of the TID-1 to TID-9 are presented in the Additional file 1: S1.

Keogram analysis

To retrieve characteristics of the observed waves, longitudinally (latitudinally) sliced images at a fixed latitude (longitude) are plotted as a function of time, which is a keogram. Figure 8 presents the keogram with the longitudinal cut (55–80°W) at a fixed latitude 35°S (upper

panel) and the latitudinal cut (20–50°S) at a fixed longitude 70°W (lower panel) as a function of time in UT. The observed TIDs (-1 to -7) are marked in the figure, and the blue triangles indicate the arrival of Lamb wave and the tsunami at around (45°S, 73°W). From the figure, one can notice that there are two time zones, one at 11:30–14:00 UT corresponding to the arrival of the Lamb wave, and the other at 16:00–20:00 UT when the tsunami arrived. It should be noted that the wave packets of the first group are narrow, having only one to two wave crests. On the other hand, the wave packets of the second group have several wave crests extending for more than 4 h. A similar keogram analysis was also applied for the Brazilian side (not shown here) to find out the wave packets.

Discussion

On 15 January 2022, we observed the atmospheric pressure wave (Lamb mode), tsunami, and ionospheric TIDs over the South American continent, which must be related to the Tonga volcanic eruption. The horizontal wavelengths, periods, phase speed, propagation direction, and amplitude of oscillations were calculated from the sequence of the dTEC maps. The wave characteristics are summarized in Table 1 and Figs. 3, 4, 5, 6, 7. The observed 9 TIDs have the horizontal wavelength of 330–1174 km, the period of 20–36 min, and the phase speed of 275–544 m/s. Their propagation directions are mainly 20°–40° (NE), except one toward 139° (SE) appeared at 11:30 UT. As can be seen in the dTEC keograms in Fig. 8, there are two groups of TID activities, one at the 11:30–14:00 UT, and the other at the 16:00–20:00 UT time

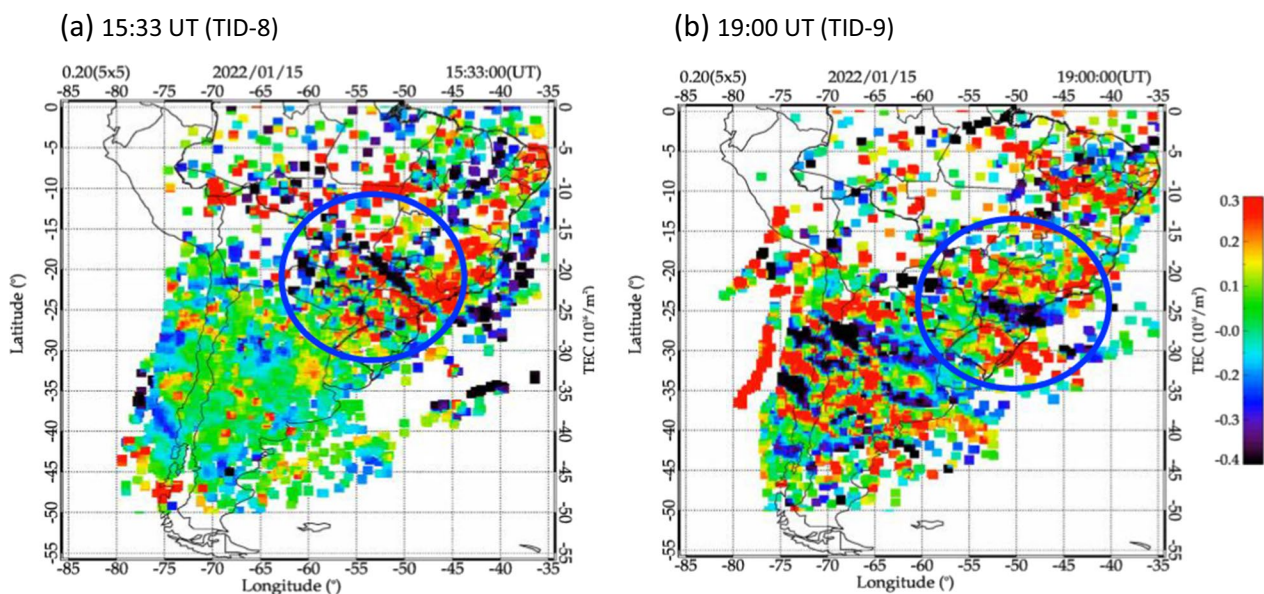


Fig. 7 Same as Fig. 3, except for (a) at 15:33 UT (TID-8) and (b) at 19:00 UT (TID-9)

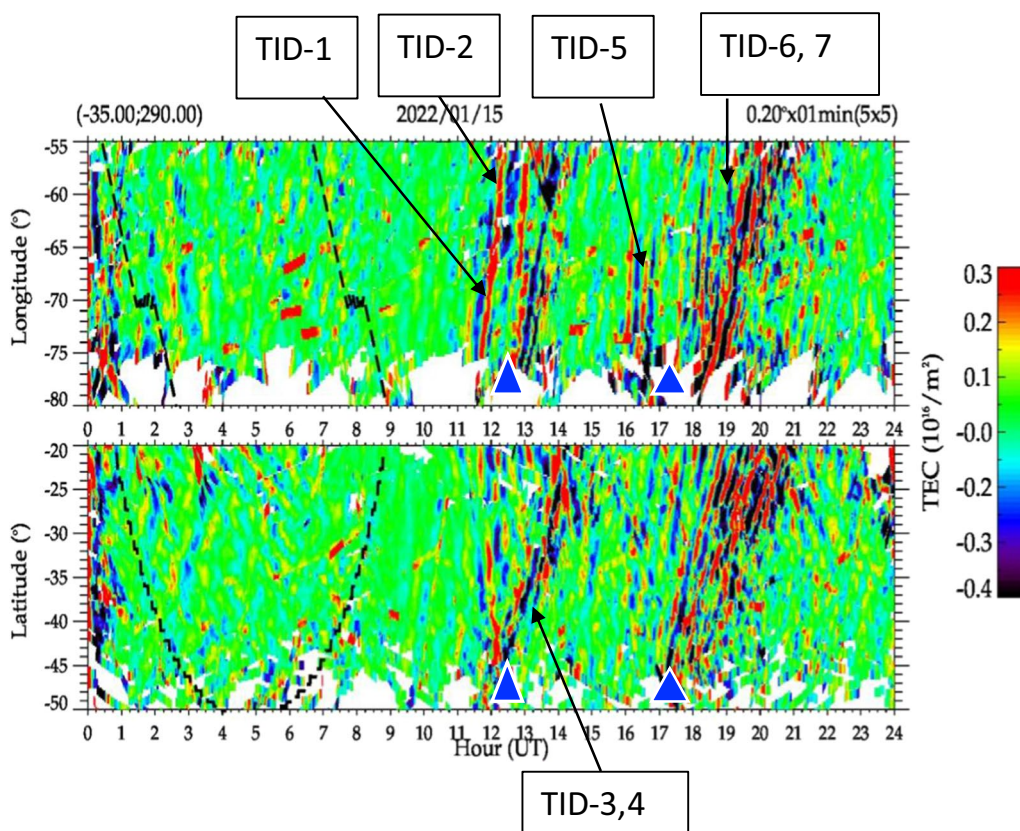


Fig. 8 Keogram of the dTEC maps of the Chile side: longitudinal cut at 35°S (upper panel) and latitudinal cut at 70°W (lower panel) as a function of time (UT) on 15 Jan 2022. The color bar shows the amplitude of dTEC oscillation. The blue triangles indicate arrival of the Lamb wave at 12:30 UT and the tsunami at 17:15 UT at Chile coast around 45°S. The broken and dashed lines indicate the sunset and sunrise time in the ionosphere at the 300 km altitude

zones. In the following section, we will try to see characteristics of the generation and propagation mechanism of these waves.

TIDs-1 to -4 (11:30–14:00 UT)

Between 11:30 UT and 14:00 UT, four TIDs passed over the Chilean coast toward the NE direction, except TID-1 which propagated toward SE. It is interesting to note that the horizontal wavelengths are gradually shorten, from 1174 to 348 km, and the phase speeds are coming to gradually slow, from 544 m/s to 294 m/s.

There are two waves TID-1 at 11:30 UT and TID-2 at 11:45 UT. They have long wavelengths (1174 and 946 km) and fast phase speeds (544 m/s and 438 m/s), one propagating toward SE and the other propagating toward NE. On the other hand, the TID-3 (12:30 UT) appeared almost simultaneously with the arrival of the Lamb wave, and the TID-4 (13:15 UT) appeared later by 45 min. The phase velocities and the propagation directions are similar to that of the Lamb wave. It seems that these 4 TIDs observed are related to the Lamb wave. However,

according to Nishida et al. (2014), Lamb wave is a confined pressure wave in the troposphere and could not induce upward wave energy flux, but a part of the oscillation leaks to thermosphere as a resonant form with periods of around 2.6 min and 4.8 min. If this is the case, Lamb wave would contribute to the excitation of short-period TIDs in the ionosphere, but not such large scale and long period (20–30 min) TIDs.

On the other hand, there has been some observational evidence of TIDs accompanied by Lamb wave propagations. Liu et al. (1982) observed almost simultaneous arrival of a surface pressure wave and the TIDs in the case of the St. Helena volcanic eruption occurred on May 18, 1980. The TIDs observed were the period of ~ 10 to 15 min and the phase speed of ~ 300 m/s. They concluded that the observed TIDs must be due to penetration of Lamb mode pressure wave into the thermosphere-ionosphere. Most recently Zhang et al. (2022) reported TIDs with a horizontal phase speed of 300–350 m/s, a period of 30–50 min, and a horizontal wavelength of 500–1000 km related to the global passage of the Lamb wave

after the Tonga eruption. Therefore, the possibility of the local excitation of TIDs by such a Lamb-mode oscillation could not be ruled out.

Another point that should be considered is that these 4 TIDs have fast phase velocities above 294 m/s. These phase speeds are faster than the speed of sound in the mesopause (80–100 km altitude). Here, we assume that the observed TIDs are generated by the propagation of local atmospheric gravity waves (Fritts et al. 2008). As pointed out by Vadas et al. (2019), the condition of propagation of a gravity wave from the mesosphere to the lower thermosphere is that the intrinsic phase speed (C_i) should be less than the local speed of sound (C_s) with the relation of $C_i/C_s < 0.9$. Although the presently observed phase speed of TID-4 is low (294 m/s), it is still faster than the speed of sound in the mesopause, which is around 260 m/s. Therefore, none of the observed TIDs was its origin from the lower atmosphere. They must be generated above the mesopause (> 100 km) as secondary waves and propagated horizontally. In this concern, Vadas et al. (2023) presented a simulation model of primary gravity waves by the Tonga volcanic eruption and subsequent generation and propagation of secondary waves in the thermosphere on a global scale. The authors mentioned that most of the gravity waves observed far from the Tonga area are likely secondary waves generated by the primary waves, but not a leakage of the Lamb wave. Whether Lamb wave or acoustic gravity waves could be a source of the observed TIDs, further investigations would be required.

TIDs-5 to -7 (16:00–20:00 UT)

The TID-5 (16:05 UT), shown in Fig. 5, appeared by one hour earlier than the arrival of the tsunami (17:15 UT), having a long wavelength (875 km) and a fast speed (470 m/s). On the other hands, the TID-6 (17:35 UT), presented in Fig. 6, appeared almost simultaneously with the arrival of the tsunami (17:15 UT). Then, TID-7 (18:35 UT) appeared by one hour later (Fig. 6). Their horizontal wavelengths are becoming shorter from 875 to 330 km. The difference of the TID-5 to -7 compared to the TID-2 to -4 seems to be the scale of wave packets. As shown in Fig. 8 (keograms) the TID-2 to -4 have only one to two crests. On the other hand, the TID-5 to -7 have several crests. It looks that the two groups of TIDs have different excitation processes.

It seems that tsunamis produce a variety of gravity waves with different horizontal wavelength and phase speeds. TIDs prior to tsunamis were simulated by Inchin et al. (2020). They found that the leading wave has a longer wavelength and faster phase speed. During the Tohoku Earthquakes on 11 March 2011, strong tsunamis were excited. Makela et al. (2011) observed the

ionospheric wave structure by OI 630 nm airglow imager at Hawaii islands after the earthquake that preceded the tsunami by approximately 1 h. Smith et al. (2015) reported for the same event that there was no measurable time difference between the tsunami arrival and the TID event observed at El Leoncito (Andes Mountains). Further, Azeem et al. (2017) reported that the TID event over the North America occurred after the arrival of the tsunami on the coast of California. From the GW simulation model, Vadas et al. (2015) derived the atmospheric acoustic and gravity waves excited by an ocean surface wave packet with a specific frequency and duration. The authors concluded that if an ocean wave packet has a sum period longer than 10–12 min, then the excited GWs could have much faster horizontal phase speeds than that of the ocean wave, and thus reach a fixed location well before the ocean wave packet. Our present results, varying the horizontal wavelength and the phase speed from TID-5 (875 km and 470 m/s) to TID-7 (330 km and 275 m/s), could be explained by the recent simulation models (Vadas et al. 2015; Inchin et al. 2020).

Effect of geomagnetic activity

From the evening of 14 to the early morning of 15 January 2022, a moderate geomagnetic activity ($K_p \sim 4-5$) was going on. The main phase ($Dst \sim -90$ nT) was around 23:00 UT on 14 January 2022. It was during the recovery phase when the Tonga eruption occurred. During the time zone of 11:00 to 20:00 UT, the K_p index varied from 4 to 2, the Dst index varied from -55 to -17 nT. The auroral activity (AE index) was less than 500 nT, except in the time zone of 13:30–14:00 UT when it was larger than 500 nT. Looking into the keogram of dTEC (Fig. 8), there are some dTEC disturbances in the period of 00:00 to 04:00 UT, which might be related to the geomagnetic activity. The TID-1 (11:30 UT), which is the longest (1174 km) and the fastest (544 m/s) wave in our present data is only one which has the different direction of propagation toward SE. Although the AE index was moderate, a possibility of generation of LSTID by the auroral activity at around 11:00 UT could not be ruled out.

Conclusions

We observed a strong atmospheric pressure wave (Lamb mode), tsunami, and 9 distinct TID wave packets in the ionosphere over South America from 11:00 to 20:00 UT on 15 January 2022, which should be related to the Tonga volcanic eruption in the South Pacific Ocean occurred at 04:15 UT on the same day. The TIDs have the horizontal wavelength of 330–1174 km, the period of 20–36 min, the phase speed of 275–544 m/s, and the propagation direction of $20^\circ-40^\circ N$, except one toward SE. Two groups of TIDs were observed, i.e., one (11:30–13:15 UT) is

before and after the arrival of the Lamb wave and the other (16:00–18:35 UT) is before and after the arrival of tsunami. Each group of TIDs appeared with a longer wavelength then becoming shorter ones. These observational results are the first time reported from the South American continent. Whether the observed TIDs are generated by the locally travelling Lamb wave or generated by secondary gravity waves far from the observation sites was not clear in the present work. Further simulation study would be necessary to understand the simultaneous occurrence of the Lamb wave at the surface and disturbances in the ionosphere.

Abbreviations

Dst	Disturbance storm time index
dTEC	Detrended total electron content
GNSS	Global navigation satellite system
IBGE	Instituto Brasileiro de Geografia e Estatística
Kp	Geomagnetic planetary index
LSTID	Large scale travelling ionospheric disturbance
MSTID	Medium scale travelling ionospheric disturbance
NOAA	National Oceanic and Atmospheric Administration
RBMC	Rede brasileiro de monitoramento contínuo
TEC	Total electron content
TID	Travelling ionospheric disturbance
UNESCO	United Nations Educational, Scientific and Cultural Organization

Supplementary Information

The online version contains supplementary material available at <https://doi.org/10.1186/s40623-023-01844-1>.

Additional file 1 (S1). Ionospheric detrended map movie over South America on 15 January 2022.

Acknowledgements

We thank the Brazilian Ministry of Science, Technology and Innovation (MCTI) and the Brazilian Space Agency (AEB) who supported the present work under the grants PO 20VB.0009. The present work was also supported by CNPq (Conselho Nacional de Pesquisa e Desenvolvimento) under the grants 310927/2020-0, 140401/2021-0, 163874/2021-2, 300322/2022-4, 150261/2022-5, 300264/2022-4; Fundação de Amparo à Pesquisa do Estado de São Paulo (FAPESP) under the grants 2018/09066-8 and 2019/22548-4; and Coordenação de Aperfeiçoamento de Pessoal de Nível Superior (CAPES) under the process 88887.514072/2020-00. Y. Otsuka was supported by JSPS KAKENHI Grant (20H00197, 21H04518), JSPS Bilateral Joint Research Projects (JPJSBP120226504), and JSPS Core-to-Core Program, B. Asia-Africa Science Platforms. L. C. A. Resende would like to thank the China-Brazil Joint Laboratory for Space Weather (CBJLSW), National Space Science Center (NSSC), Chinese Academy of Sciences (CAS) for supporting her postdoctoral.

Author contributions

HT was responsible for data analysis, interpretation and text editing. CAOBF was responsible for data analysis and interpretation, DB contributed for data analysis, CM Wrasse contributed for data analysis and interpretation, GAG, RHH and LFRV contributed to data analysis, LCA Resende contributed to data analysis and interpretation, PKN, TTA, CSC and MBP contributed to data collection and analysis and YO contributed to data interpretation and discussion. All authors read and approved the final manuscript.

Funding

The authors contributed in the present work under being supported by the following institutions, Brazilian Ministry of Science, Technology and Innovation (MCTI), Brazilian Space Agency (AEB), Conselho Nacional de Pesquisa e

Desenvolvimento (CNPq), Fundação de Amparo à Pesquisa do Estado de São Paulo (FAPESP), Coordenação de Aperfeiçoamento de Pessoal de Nível Superior (CAPES), Japanese Society of Promotion of Science (JSPS), China-Brazil Joint Laboratory for Space Weather (CBJLSW).

Availability of data and materials

GNSS ground-based receiver data, used in the present study, are available from IBGE (Instituto Brasileiro de Geografia e Estatística) at: <https://www.ibge.gov.br/geociencias/informacoes-sobre-posicionamento-geodesico/rede-geodesica/16258-rede-brasileira-de-monitoramento-contínuo-dos-sistemas-gnss-rbmc.html?=&t=o-que-e>. The atmospheric pressure data in Chile are available from DGAC (Direção Meteorológica do Chile) at < <https://climatologia.meteochile.gob.cl/> >. The ocean sea level data are available from the Sea level observing system/UNESCO at the site: < <http://www.ioc-sealevelmonitoring.org/index.php> >. The tsunami simulation data are available at IRiDeS (International Research Institute of Disaster Science, Tohoku university, Japan), at the site: < https://irides.tohoku.ac.jp/research/prompt_investigation/2022_tonga-vol-tsunami.html >.

Declarations

Ethics approval and consent to participate

Not applicable.

Competing interests

The authors have no competing interests with any other groups.

Author details

¹Instituto Nacional de Pesquisas Espaciais, São José dos Campos, Brazil. ²State Key Laboratory of Space Weather, Beijing, China. ³Institute for Space-Earth Environmental Research, Nagoya University, Nagoya, Japan.

Received: 20 December 2022 Accepted: 8 May 2023

Published online: 25 May 2023

References

- Adam D (2022) Tonga volcano created puzzling atmospheric ripples. *Nature* 602:3. <https://doi.org/10.1038/d41586-022-00127-1>
- Astafyeva E (2019) Ionospheric detection of natural hazards. *Rev Geophys.* 57:1265–1288. <https://doi.org/10.1029/2019RG000668>
- Azeem I, Vadas SL, Crowley G, Makela JJ (2017) Traveling ionospheric disturbances over the United States induced by gravity waves from the 2011 Tohoku tsunami and comparison with gravity wave dissipative theory. *J Geophys Res Space Phys.* <https://doi.org/10.1002/2016JA023659>
- Duncombe J (2022) The surprising reach of Tonga's giant atmospheric waves. *Eos.* <https://doi.org/10.1029/2022EO220050>
- Figueiredo CAO, Takahashi H, Wrasse CM, Otsuka Y, Shiokawa K, Barros D (2018) Medium-scale traveling ionospheric disturbances observed by detrended total electron content maps over Brazil. *J Geophys Res Space Physics* 123:2215–2227. <https://doi.org/10.1002/2017JA025021>
- Fritts DC, Vadas SL, Riggan DM, Abdu MA, Batista IS, Takahashi H et al (2008) Gravity wave and tidal influences on equatorial spread F based on observations during the spread F experiment (SpreadFEx). *Annal Geophys* 26(11):3235–3252. <https://doi.org/10.5194/angeo-26-3235-2008>
- Inchin PA, Heale CJ, Snively JB, Zettergren MD (2020) The dynamics of non-linear atmospheric acoustic-gravity waves generated by tsunamis over realistic bathymetry. *J Geophys Res Space Phys.* <https://doi.org/10.1029/2020JA028309>
- Komjathy A, Yang Y-M, Meng X, Verkhoglyadova O, Mannucci AJ, Langley RB (2016) Review and perspectives: understanding natural-hazards-generated ionospheric perturbations using GPS measurement and coupled modeling. *Radio Sci* 51:951–961. <https://doi.org/10.1002/2015RS005910>
- Kubota T, Saito T, Nishida K (2022) Global fast-traveling tsunamis by atmospheric pressure waves on the 2022 Tonga eruption. *Science* 377(6601):91–94. <https://doi.org/10.1126/science.abo4364>
- Lin J-T, Rajesh PK, Lin CCH, Chou M-Y, Liu J-Y, Yue J et al (2022) Rapid conjugate appearance of the giant ionospheric Lamb wave signatures in the

- northern hemisphere after Hunga-Tonga volcano eruptions. *Geophys Res Lett* 49:e2022GL098222. <https://doi.org/10.1029/2022GL098222>
- Lindzen RS, Blake D (1972) Lamb waves in the presence of realistic distributions of temperature and dissipation. *J Geophys Res* 77:2166–2176. <https://doi.org/10.1029/JC077i012p02166>
- Liu CH, Klostermeyer J, Yeh KC, Jones TB, Robinson T, Holt O, Leitingner R, Ogawa T, Sinno K, Kato S, Ogawa T, Bedard AJ, Kersley L (1982) Global dynamic responses of the atmosphere to the eruption of Mount St. Helens on 18 May 1980. *J Geophys Res* 87(A8). <https://doi.org/10.1029/JA087iA08p06281>
- Makela JJ et al (2011) Imaging and modeling the ionospheric airglow response over Hawaii to the tsunami generated by the Tohoku earthquake of 11 March 2011. *Geophys Res Lett* 38:L13305. <https://doi.org/10.1029/2011GL047860>
- Matoza RS et al (2022) Atmospheric waves and global seismoacoustic observations of the January 2022 Hunga eruption, Tonga. *Science* 377(6601):95–100. <https://doi.org/10.1126/science.abo7063>
- Nishida K, Kobayashi N, Fukao Y (2014) Background Lamb waves in the Earth's atmosphere. *Geophys J Int* 196:312–316. <https://doi.org/10.1093/gji/ggt413>
- Otsuka Y, Suzuki K, Nakagawa S, Nishioka M, Shiokawa K, Tsugawa T (2013) GPS observations of medium-scale traveling ionospheric disturbances over Europe. *Ann Geophys* 31:163–172. <https://doi.org/10.5194/angeo-31-163-2013>
- Smith SM, Martinis CR, Baumgardner J, Mendillo M (2015) All-sky imaging of transglobal thermospheric gravity waves generated by the March 2011 Tohoku Earthquake. *J Geophys Res Space Phys* 120:10992–10999. <https://doi.org/10.1002/2015JA021638>
- Themens DR, Watson C, Žagar N, Vasylykevych S, Elvidge S, McCaffrey A et al (2022) Global propagation of ionospheric disturbances associated with the 2022 Tonga volcanic eruption. *Geophys Res Lett* 49:e2022GL098158. <https://doi.org/10.1029/2022GL098158>
- Tsugawa T, Saito A, Otsuka Y, Nishioka M, Maruyama T, Kato H, Nagatsuma T, Murata KT (2011) Ionospheric disturbances detected by GPS total electron content observation after the 2011 off the Pacific coast of Tohoku Earthquake. *Earth Planets Space* 63:875–879. <https://doi.org/10.5047/eps.2011.06.035>
- Vadas SL, Makela JJ, Nicolls MJ, Milliff RF (2015) Excitation of gravity waves by ocean surface wave packets: upward propagation and reconstruction of the thermospheric gravity wave field. *J Geophys Res Space Phys*. <https://doi.org/10.1002/2015JA021430>
- Vadas SL, Xu S, Yue J, Bossert K, Becker E, Baumgarten G (2019) Characteristics of the quiet-time hot spot gravity waves observed by GOCE over the Southern Andes on 5 July 2010. *J Geophys Res Space Phys* 124(8):7034–7061. <https://doi.org/10.1029/2019JA026693>
- Vadas SL, Becker E, Figueiredo C, Bossert K, Harding KB, Claire Gasque LC (2023) Primary and secondary gravity waves and large-scale wind changes generated by the Tonga volcanic eruption on 15 January 2022: modeling and comparison with ICON-MIGHTI winds. *J Geophys. Res. Space Physics* 128(2):e2022JA031138. <https://doi.org/10.1029/2022JA031138>
- Wright CJ, Neil Hindley M, Alexander J et al (2022) Tonga eruption triggered waves propagating globally from surface to edge of space. *ESS Open Arch*. <https://doi.org/10.1002/essoar.10510674.1>
- Zhang S-R, Vierinen J, Aa E, Goncharenko LP, Erickson PJ, Rideout W, Coster AJ, Spicher A (2022) 2022 Tonga Volcanic Eruption Induced Global Propagation of Ionospheric Disturbances via Lamb Waves. *Front Astron Space Sci*. 9:871275. <https://doi.org/10.3389/fspas.2022.871275>

Publisher's Note

Springer Nature remains neutral with regard to jurisdictional claims in published maps and institutional affiliations.

Submit your manuscript to a SpringerOpen[®] journal and benefit from:

- Convenient online submission
- Rigorous peer review
- Open access: articles freely available online
- High visibility within the field
- Retaining the copyright to your article

Submit your next manuscript at ► [springeropen.com](https://www.springeropen.com)
